Economically sustainable bifunctional Ni@C catalyst in a solar-to-hydrogen device employing a CIGS submodule

Quang-Tung Ngo[a,‡], Oleksii Omelianovych[a,‡], Van-Toan Nguyen[a], Byung Tae Ahn[b], Kyu-Bock Lee[c], Gyoung-Ja Lee[d], Liudmila L. Larina[a,e*] and Ho-Suk Choi[a*]

[a]Department of Chemical Engineering and Applied Chemistry, Chungnam National University, Yuseong-Gu, Daejeon 34134, Republic of Korea

[b]Department of Material Science and Engineering, Korea Advanced Institute of Science and Technology, Daejeon 34141, Republic of Korea

[c]Graduate School of Energy Science & Technology, Chungnam National University, Yuseong-Gu, Daejeon 34134, Republic of Korea

[d]Smart Structural Safety and Prognosis Research Division, Korea Atomic Research Institute, Yuseong-gu, Daejeon 305353, Republic of Korea

[e]Department of Solar Photovoltaics, Institute of Biochemical Physics, Russian Academy of Sciences, Kosygin St. 4, 119334, Moscow, Russia

‡These authors contributed equally

*Corresponding authors:

llarina3333@cnu.ac.kr (Liudmila L. Larina); hchoi@cnu.ac.kr (Ho-Suk Choi)
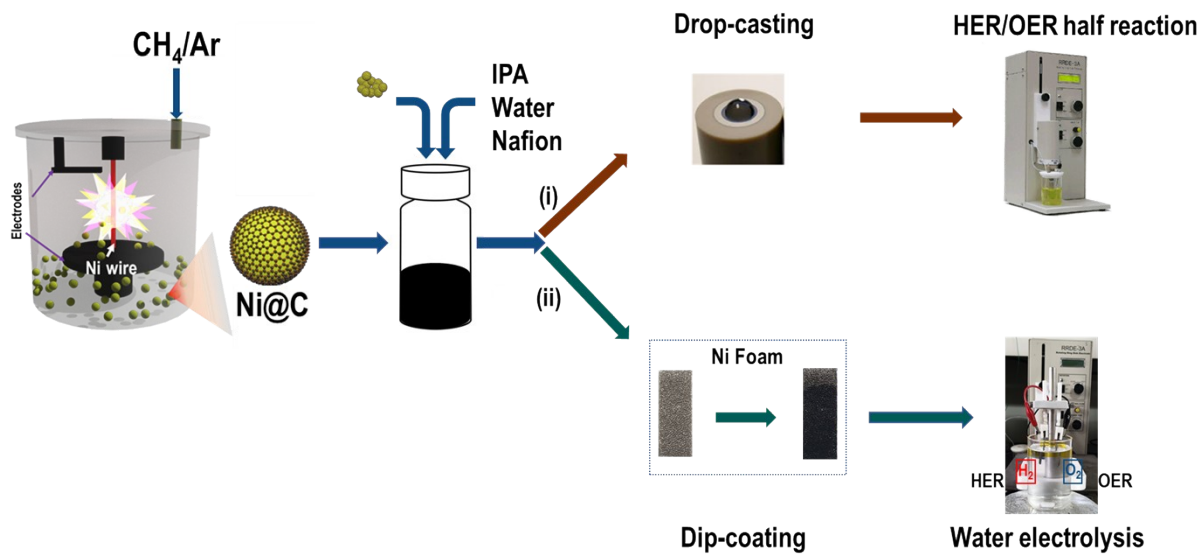
Scheme S1. Synthesis procedure of Ni@C core@shell nanoparticles and fabrication process of the electrodes for the electrochemical experiments
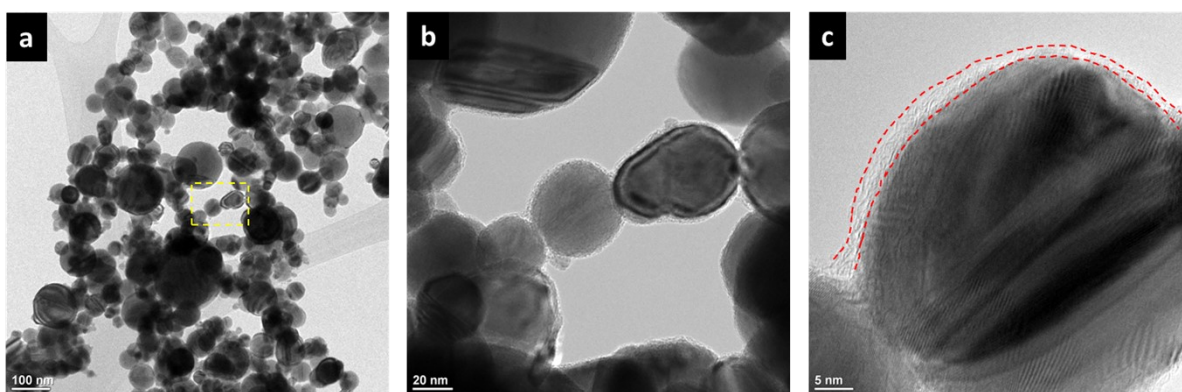
Figure S1. (a-c) Different magnification HRTEM images of Ni@C(0%). Shell feature is highlighted with dash-line of red color.
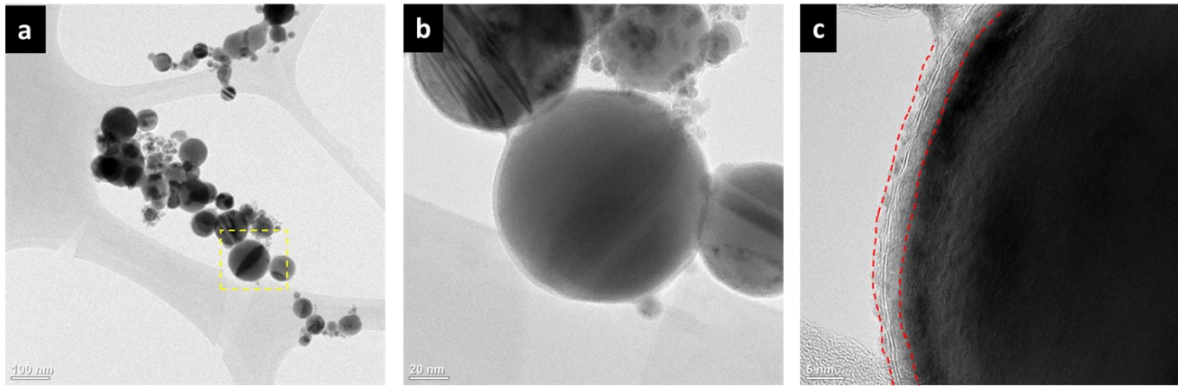
Figure S2. (a-c) Different magnification HRTEM images of Ni@C(5%). Shell feature is highlighted with dash-line of red color.
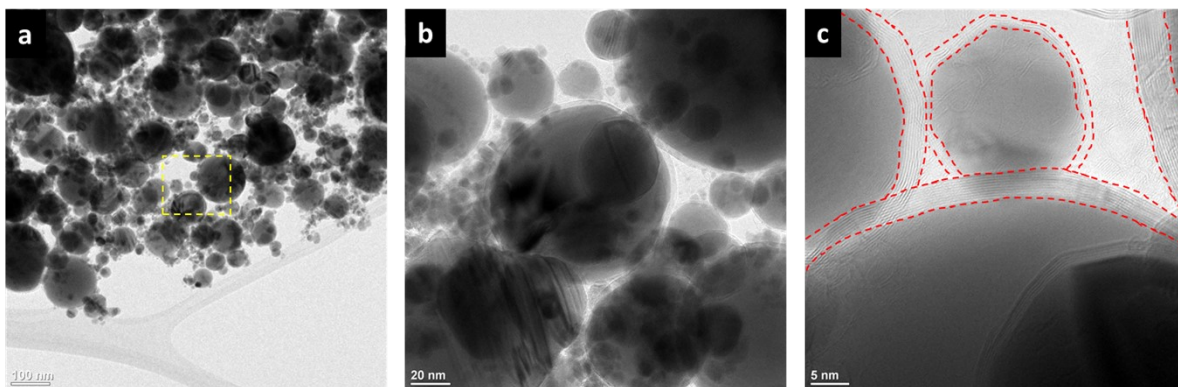
Figure S3. (a-c) Different magnification HRTEM images of Ni@C(10%). Shell feature is highlighted with dash-line of red color.
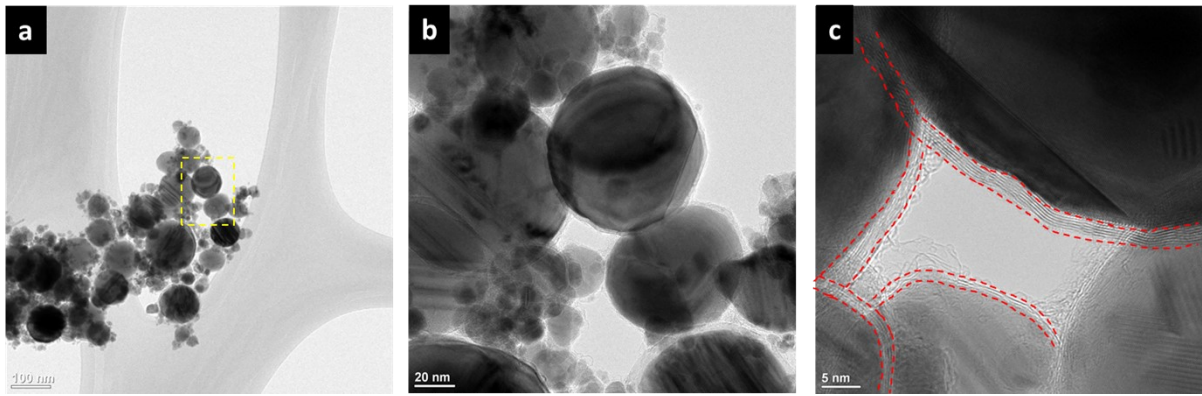
Figure S4. (a-c) Different magnification HRTEM images of Ni@C(15%). Shell feature is highlighted with dash-line of red color.
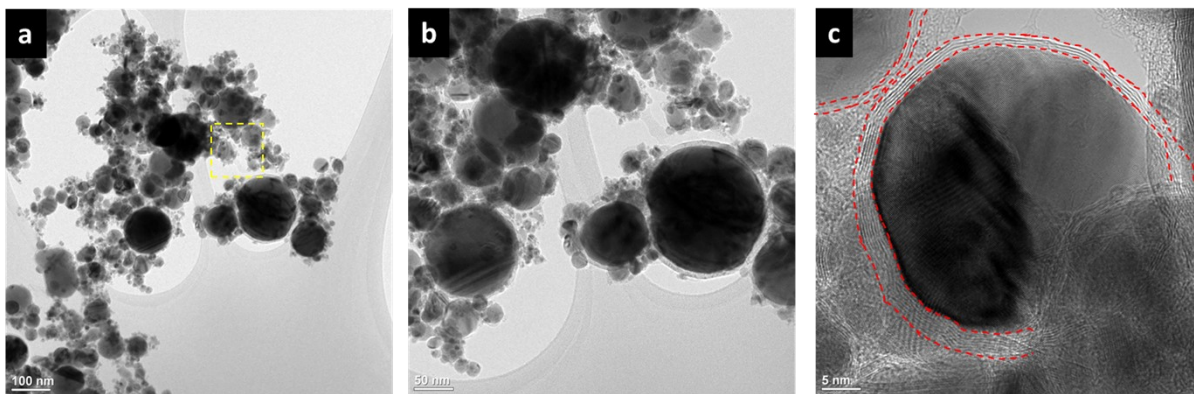
Figure S5. (a-c) Different magnification HRTEM images of Ni@C(20%). Shell feature is highlighted with dash-line of red color.

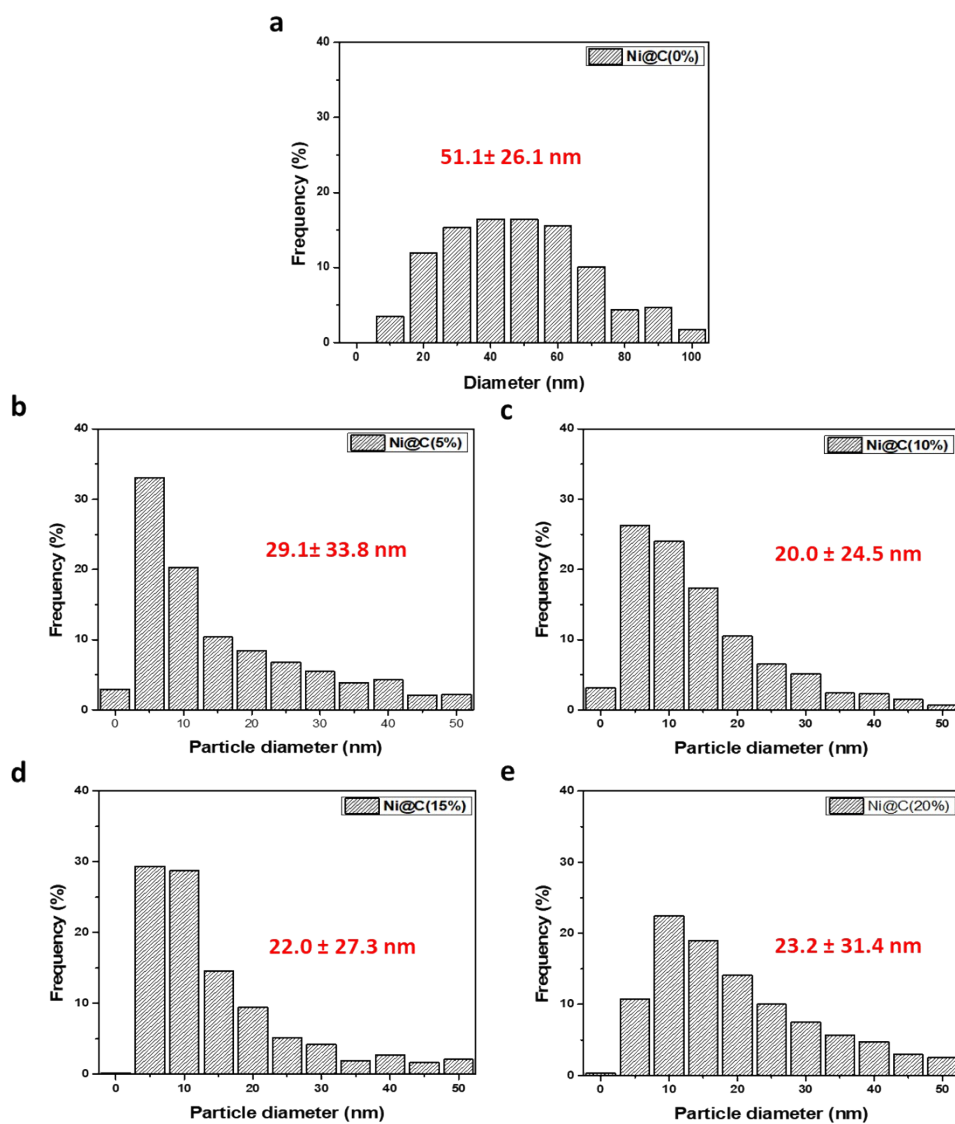**Figure S6.** Particle size distribution of **(a)** Ni@C(0%), **(b)** Ni@C(5%), **(c)** Ni@C(10%), **(d)** Ni@C(15%) and **(e)** Ni@C(20%). The numbers on the figures represent average particle diameter ± standard deviation.

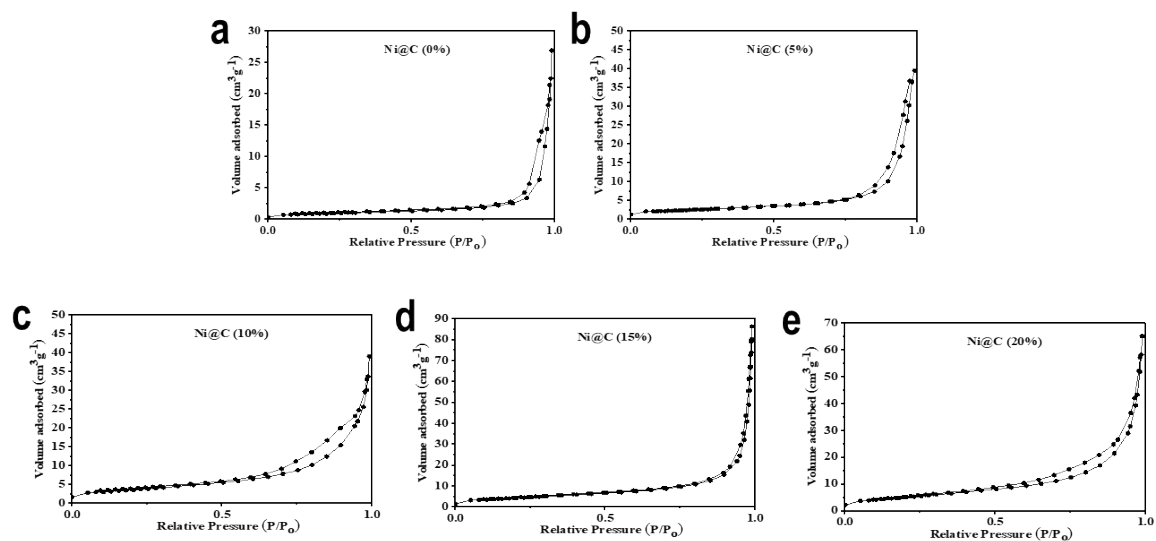**Figure S7.** Nitrogen adsorption-desorption isotherms recorded for the **(a)** Ni@C(0%), **(b)** Ni@C(5%), **(c)** Ni@C(10%), **(d)** Ni@C(15%), and **(e)** Ni@C(20%) catalysts
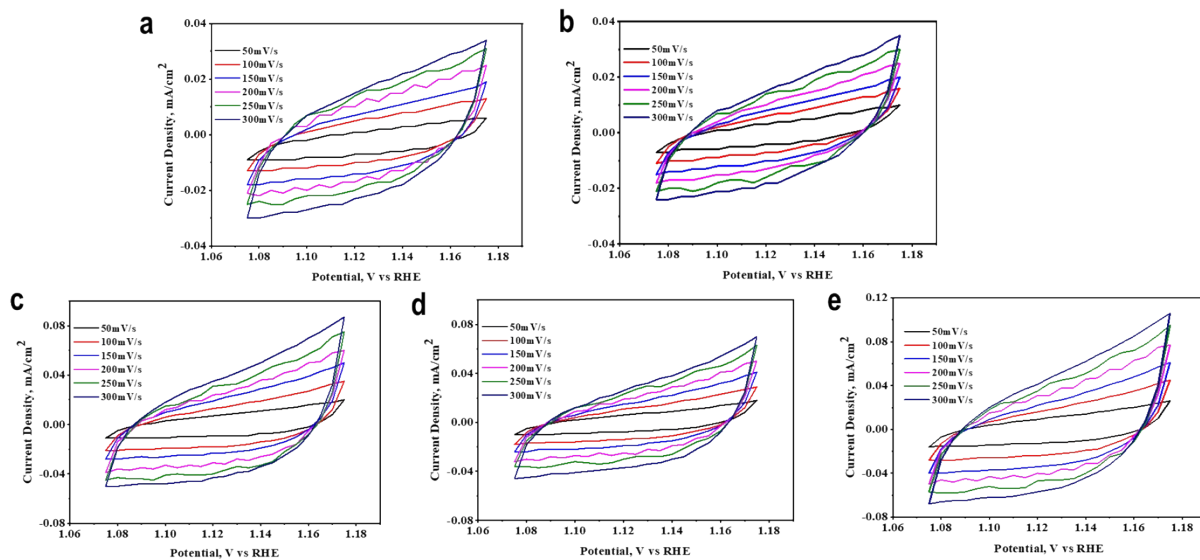
Figure S8. Cyclic voltammetry curves with different scan rates recorded for the (a) Ni@C(0%), (a) (b) Ni@C(5%), (c) Ni@C(10%), (d) Ni@C(15%), and (e) Ni@C(20%) catalysts
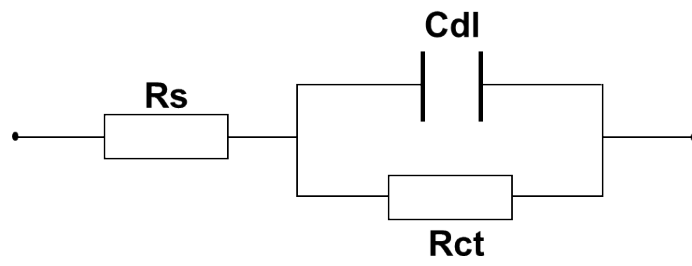
Figure S9. Equivalent circuit scheme for the EIS analysis

Table S1. Active Surface Area and Total Pore Volume Values Obtained from a BET Analysis of the Ni@C(x%) Catalysts (x = 0, 5%, 10%, 15%, and 20%)

Catalysts	Ni@C(0%)	Ni@C(5%),	Ni@C(10%)	Ni@C(15%)	Ni@C(20%)
BET area, m^2g^{-1}	3.23	8.69	12.65	15.13	18.18
Total pore volume, cm^3g^{-1}	0.040	0.061	0.055	0.127	0.098

Construction of the Solar-to-Hydrogen System

The CIGS module captures sunlight and converts it into electricity, directly feeding the electrochemical water-splitting unit. The negative terminal of the CIGS module was directly connected to the anode (OER) of the electrolyzer. The counter electrode port of the potentiostat connected to the reference port (for a two-electrode configuration) was then connected to the cathode (HER) of the electrolyzer. Finally, to complete the circuit, the working electrode port of the potentiostat was connected to the cathode of the CIGS module. The current of the water-splitting cell was recorded by chronoamperometry for different time intervals under AM 1.5G illumination without applying any external bias.
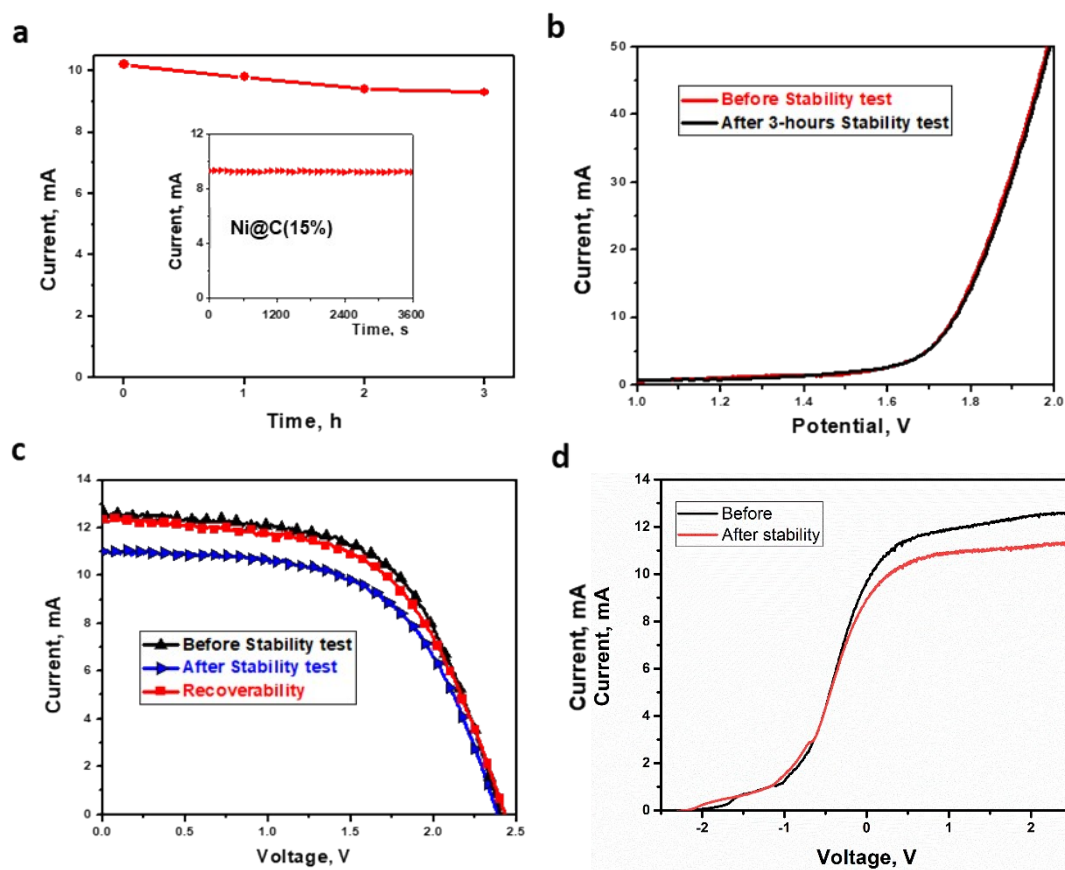
Stability

Figure S10. The stability test: (a) Photocurrent–time curve of the integrated CIGS-4 device without external bias under steady-state illumination. (b) LSV polarization curve of the Ni@C(15%) catalyst for overall water splitting in a two-electrode configuration in 1M KOH. (c) J–V characteristics of the CIGS-4 sub-module before the stability test, after the stability test (three hours), and recoverability of the CIGS-4 sub-module 12 hours after the stability test. (d) Photocurrent–voltage curves of the integrated water-splitting device

For actual applications of a PV-driven water-splitting system, stability is a crucial issue. In order to clarify the long-term operation effects on the system performance, we carried out stability tests. We found that the current decreases continuously during long-term operation. The gradient, however, is not constant. The current decreased by 0.4 mA after each of the first two consecutive hours of the measurements. Importantly, during the third hour of operation, the value of the generated current was reduced only by 0.1 mA, indicating stabilization of the setup (Fig. S9a). Clarification of the exact cause of the current reduction was provided by analyzing the IV characteristics of the solar cell and the LSV of the water-splitting system in a disconnected state. No differences between the LSV curves before and after the stability test were found (Fig. S9b). However, there is a noticeable reduction of the photocurrent generated

14

by the CIGS sub-module after three hours of operation. The representative I-V characteristics of the device are shown in Fig. S9c. The corresponding PV parameters of the device are summarized in Table S2. Therefore, we can conclude that the leading cause of the current reduction is the instability of the cells in the CIGS sub-module. The IV curves of the integrated water-splitting device are shown in Fig. S9d. Another point for further investigation arises from the IV characteristics of the same CIGS module recorded 12 hours after the stability test. According to our data, the sub-module fully recovered during storage and shows performance similar to that recorded before the stability test (Fig. S9c, Table S2).

Table S2. Photovoltaic Parameters of CIGS-4 before the Stability Test, after the Stability Test, and Recoverability Data

PV parameters	Isc, mA	Voc, V	Pmax, mW/cm^2	FF	PCE,%
Before stability test	12.67	2.41	11.23	0.59	11.69
After stability test	11.01	2.41	9.63	0.58	9.63
Recoverability	12.33	2.43	10.74	0.57	11.17